Geophysical Journal International

Geophys. J. Int. (2015) **201,** 1142–1155 doi: 10.1093/gji/ggv046
GJI Seismology

Horizontal-to-vertical spectral ratios from a full-wavefield model of ambient vibrations generated by a distribution of spatially correlated surface sources

Enrico Lunedei and Dario Albarello

Dipartimento di Scienze Fisiche, della Terra e dell'Ambiente, Università degli Studî di Siena, Via Laterina 8, *I*-53100 *Siena, Italy. E-mail: lunedei@unisi.it*

Accepted 2015 January 26. Received 2015 January 21; in original form 2014 September 22

SUMMARY

A new effective model is presented to compute horizontal-to-vertical spectral ratios (HVSR) relative to ambient vibrations, under the assumption that these are originated by a distribution of spatially correlated random surface sources. The major novelty of this model lies in the description of both ground displacement and sources as stochastic fields defined on the Earth's surface, stationary in time and homogeneous in space. In this frame, the power spectral density of the displacement stochastic field can be written as a function of the power spectral density of the force stochastic field and of the subsoil properties, through the relevant Green's function. Spatial correlation between ambient vibration sources is shown to be a necessary condition to warrant convergence of the integrals defining the frequency power spectra of the displacement field that make up the HVSR curve. Furthermore, it is shown that this HVSR curve may be significantly affected by the effective range of the force-field correlation on the Earth's surface. This formalization reduces computational efforts with respect to the previous version of the model based on distributed surface sources and may provide synthetic HVSR-curve patterns that are in line with those given by that computationally more troublesome version, as well as with those deduced under the assumption that the ambient vibrations constitute a diffuse wavefield.

Key words: Numerical solutions; Site effects; Wave propagation.

1 INTRODUCTION

The possibility of using ambient vibration measurements to retrieve low-strain seismic properties of the subsoil relies on the possibility of developing physical models able to establish a relationship between the average properties of this field, measured at a site on the Earth's surface, and the subsoil structure at the same site. In recent years, both single-station (e.g. Tokimatsu 1997; Bard 1998) and array (e.g. Okada 2003) configurations have been considered, on purpose. In particular, concerning single-station measurements, the horizontal-to-vertical spectral ratio (HVSR) technique has become very popular for fast and cheap seismic characterization of extended areas (e.g. Albarello *et al.* 2011). Outcomes of single-station (the HVSR curve) and array (the surface wave dispersion curve) measurements are singly (e.g. Castellaro & Mulargia 2009) or jointly (e.g. Picozzi & Albarello 2007) inverted to determine the local *S*-wave velocity (V_S) profile or other significant pieces of information (e.g. Parolai 2014). A key element of such inversion protocols is the availability of effective forward models for implementation in the related numerical procedures. In principle, such models should be characterized by a sound physical basis (in that they are able to capture underlying physical processes) and computational effectiveness. These two aspects are in many cases conflicting, in that completeness of the physical model (including e.g. all the seismic phases actually present in the ambient vibration wavefield) also implies that a significant increase of computational effort is necessary to provide realistic outcomes. On the other hand, computational effectiveness generally requires the use of simplified physical models, which, in some cases, are unable to capture basic features of the underlying physical processes.

Concerning the inversion of HVSR curves, the simplest forward modelling is based on the assumption that average spectral ratios are controlled by body waves (*P* and *SH*) propagating vertically along a stack of flat, uniform, isotropic viscoelastic layers representing the crust (e.g. Herak 2008). However, this model (actually very effective computationally) does not take into account the significant contribution of surface waves to the ambient vibration wavefield, widely recognized from observations and theoretical arguments (e.g. Bonnefoy-Claudet *et al.* 2006). To account for this evidence, forward models have been provided, with the assumption that HVSR curves are entirely controlled by Rayleigh-wave ellipticity (e.g. Tokimatsu 1997). More recently, this model has been generalized to account for the presence of Love waves

and higher modes (Arai & Tokimatsu 2000, 2004; Lunedei & Albarello 2009). Theoretical modelling (Bonnefoy-Claudet *et al.* 2004, 2006, 2008; Albarello & Lunedei 2010, 2011), however, suggests that both body waves and surface waves contribute to the average HVSR-curve pattern in a way that is controlled by subsurface structure and source distribution. This implies that a realistic forward model should include all seismic phases potentially contributing to the ambient vibration wavefield.

Such a full-wavefield modelling has in fact been proposed, by considering two different theories. In the earlier model, ambient vibrations are assumed to be the effect of a distribution of aleatory uncorrelated point-like forces lying on the Earth's surface or close to it (e.g. Field & Jacob 1993; Lanchet & Bard 1994; Arai & Tokimatsu 2004). The last version of this theory (Lunedei & Albarello 2010) will be hereafter referred to as the distributed surface sources (DSS) model. More recently, Sánchez-Sesma *et al.* (2011) proposed a new approach, named the diffuse field approach (DFA), for modelling HVSR, where the ambient vibrations are assumed to be a diffuse wavefield.

The two models are not equivalent in terms of underlying physical hypotheses but provide similar outcomes (see e.g. García-Jerez *et al.* 2012). From the computational point of view, however, the DFA model is much faster than the DSS model in computing synthetic HVSR curves. This is because the DSS model requires a double integration (Lunedei & Albarello 2010): in wavenumber and in source–receiver distance. As the DFA model only needs a single integration (in the wavenumber domain), the run time is approximately quadratically inferior.

Besides the practical aspect of computational effectiveness, there are also two key theoretical drawbacks of the DSS model in the formulations proposed so far. The first concerns the convergence of the double generalized integrals (eqs 45–47 of Lunedei & Albarello 2010) representing the displacement frequency power-spectra that make up the HVSR curve. Their convergence was assumed as a hypothesis in Lunedei & Albarello (2010), since this property was hardly valuable in that context. Nevertheless, we will show in the present work that these integrals actually do not converge. The second problematic theoretical aspect of the DSS model has a more physical nature and significance. The assumption that the surface sources are mutually spatially uncorrelated, irrespective of their relative distance and wavelength of concern, is a physically unrealistic limitation.

In the following, a new formulation of the DSS model will be presented that allows us to overcome all the above limitations. In particular, a new representation of distributed surface sources in the form of a spatially correlated stochastic field is introduced. This new representation allows reduction of computational efforts (a single integration, in the wavenumber domain, is requested) and the assumption of source-to-source non-correlation is released. In this way, the DSS and DFA models become computationally equivalent and discussion can focus on the respective outcomes. To this purpose, synthetic HVSR curves deduced from DSS and DFA models relative to a benchmark subsoil configuration will be compared, along with those provided by previous approximate models. An example from a real site is also considered, in order to show the capability of this new model to reproduce an experimental HVSR curve.

2 DISPLACEMENT AND FORCE FIELDS AS HOMOGENEOUS STOCHASTIC FIELDS

In the following, only the vertical heterogeneity in the mechanical properties of the subsoil is taken into account, i.e. the Earth is approximated as a stack of horizontal flat viscoelastic homogeneous and isotropic layers overlying a half-space with analogous properties. On the Earth's surface, i.e. the plane described by the Cartesian vector $\mathbf{x} \equiv (x, y)^{\mathrm{T}}$, the ambient vibration displacement field,

$$\mathbf{U}(x, y, t) = \begin{pmatrix} U_x(x, y, t) \\ U_y(x, y, t) \\ U_z(x, y, t) \end{pmatrix} \in \mathbb{R}^3,$$

and the force field that generates it,

$$\mathbf{F}(x, y, t) = \begin{pmatrix} F_x(x, y, t) \\ F_y(x, y, t) \\ F_z(x, y, t) \end{pmatrix} \in \mathbb{R}^3,$$

are established as random fields, t being the time. They are both three-variate (they have three Cartesian components) and three-dimensional (they depend on three variables) and are assumed to be stationary in time t and homogeneous in horizontal position $\mathbf{x}$ (both at least at second order), with zero mean and finite variance.

Since ambient vibration displacements are assumed to be small, a linear relationship can be assumed to link the displacement and the force stochastic fields:

$$U_i(x, y, t) = \sum_{j=x,y,z} \int_{\mathbb{R}^3} G_{ij}(\xi, \eta, \tau) \cdot F_j(x - \xi, y - \eta, t - \tau)\ \mathrm{d}\xi\, \mathrm{d}\eta\, \mathrm{d}\tau\ , \tag{1}$$

for $i = x, y, z$, G_{ij} being the component along the ith direction of the Green's function, relative to the force component along the jth direction.

Furthermore, it is assumed that power spectral density functions exist for both fields, which are represented by the respective spectral matrices,

$$\mathbf{h}_\bullet(k_x, k_y, \omega) = \begin{pmatrix} h_{\bullet,xx}(k_x, k_y, \omega) & h_{\bullet,xy}(k_x, k_y, \omega) & h_{\bullet,xz}(k_x, k_y, \omega) \\ h_{\bullet,yx}(k_x, k_y, \omega) & h_{\bullet,yy}(k_x, k_y, \omega) & h_{\bullet,yz}(k_x, k_y, \omega) \\ h_{\bullet,zx}(k_x, k_y, \omega) & h_{\bullet,zy}(k_x, k_y, \omega) & h_{\bullet,zz}(k_x, k_y, \omega) \end{pmatrix},$$

where '$\bullet$' stands for U or F, respectively, when the displacement or the force fields are considered. Diagonal and off-diagonal terms respectively represent auto-spectra and cross-spectra of the corresponding field components. All of them depend on the angular frequency ω and on the 2-D wavenumber vector $\mathbf{k} \equiv (k_x, k_y)^{\mathrm{T}}$, corresponding to the time (t) and the horizontal position ($\mathbf{x} \equiv (x, y)^{\mathrm{T}}$), respectively. Due to eq. (1), one has

$$\mathbf{h}_U(k_x, k_y, \omega) = \widehat{\mathbf{G}}(k_x, k_y, \omega) \cdot \mathbf{h}_F(k_x, k_y, \omega) \cdot \widehat{\mathbf{G}}^*(k_x, k_y, \omega) \tag{2}$$

(e.g. Priestley 1981; Vanmarcke 2010), where '*' stands for the Hermitian conjugation and

$$\widehat{\mathbf{G}}(k_x, k_y, \omega) = \begin{pmatrix} \widehat{G}_{xx}(k_x, k_y, \omega) & \widehat{G}_{xy}(k_x, k_y, \omega) & \widehat{G}_{xz}(k_x, k_y, \omega) \\ \widehat{G}_{yx}(k_x, k_y, \omega) & \widehat{G}_{yy}(k_x, k_y, \omega) & \widehat{G}_{yz}(k_x, k_y, \omega) \\ \widehat{G}_{zx}(k_x, k_y, \omega) & \widehat{G}_{zy}(k_x, k_y, \omega) & \widehat{G}_{zz}(k_x, k_y, \omega) \end{pmatrix}, \tag{3}$$

is the Green's matrix in the wavenumber–frequency domain. The entries of this matrix are the Fourier transforms of the corresponding entries of the Green's matrix in the space–time domain:

$$\widehat{G}_{ij}(k_x, k_y, \omega) = \int_{\mathbb{R}^3} G_{ij}(x, y, t) \cdot \mathrm{e}^{\mathrm{i}(k_x x + k_y y + \omega t)} \, \mathrm{d}x \, \mathrm{d}y \, \mathrm{d}t \, ,$$

for $i, j = x, y, z$.

Another assumption is that the three Cartesian components of the force field are uncorrelated with one another. This implies that all the cross-spectra are zero and the force spectral matrix is diagonal:

$$\mathbf{h}_F(k_x, k_y, \omega) = \mathrm{diag}\left(h_{F,xx}(k_x, k_y, \omega), h_{F,yy}(k_x, k_y, \omega), h_{F,zz}(k_x, k_y, \omega)\right).$$

Under this assumption, eq. (2) gives a compact formula for the auto-spectrum of the ith ($i = x, y, z$) displacement component:

$$h_{U,ii}(k_x, k_y, \omega) = \sum_{j=x,y,z} \left|\widehat{G}_{ij}(k_x, k_y, \omega)\right|^2 \cdot h_{F,jj}(k_x, k_y, \omega). \tag{4}$$

In light of this result, the spectral power of the ambient vibration displacement along the ith ($i = x, y, z$) direction at each angular frequency ω (which is the marginal power spectral density function with respect to the frequency, e.g. Vanmarcke 2010) can be computed by the formula

$$\begin{aligned} \widetilde{h}_{U,i}(\omega) &= \frac{1}{(2\pi)^2} \cdot \int_{\mathbb{R}^2} h_{U,ii}(k_x, k_y, \omega) \, \mathrm{d}k_x \, \mathrm{d}k_y \\ &= \frac{1}{(2\pi)^2} \cdot \int_{\mathbb{R}^2} \sum_{j=x,y,z} \left|\widehat{G}_{ij}(k_x, k_y, \omega)\right|^2 \cdot h_{F,jj}(k_x, k_y, \omega) \, \mathrm{d}k_x \, \mathrm{d}k_y \\ &= \sum_{j=x,y,z} \mathfrak{h}_{ij}(\omega), \end{aligned} \tag{5}$$

where, for $i, j = x, y, z$,

$$\mathfrak{h}_{ij}(\omega) \equiv \frac{1}{(2\pi)^2} \cdot \int_{\mathbb{R}^2} \left|\widehat{G}_{ij}(k_x, k_y, \omega)\right|^2 \cdot h_{F,jj}(k_x, k_y, \omega) \, \mathrm{d}k_x \, \mathrm{d}k_y. \tag{6}$$

The final assumption is that the force field is isotropic in the wavenumber plane, i.e. its power spectral density function does not depend on the wavenumber-vector direction. Passing to a polar coordinate system, where the wavenumber vector is defined by its modulus k and argument ϕ, this last assumption implies that the force power spectral density function can be redefined as a function of two variables only: $h_{F,jj}(k, \omega)$, $j = x, y, z$. Under this hypothesis, the frequency power-spectrum components in eq. (6) become integrals with respect to the wavenumber modulus only, in the form given in Appendix A. As a consequence, the displacement frequency power spectra in eq. (5) become

$$\begin{aligned} \widetilde{h}_{U,x}(\omega) = \frac{1}{16\pi} \cdot \int_0^{+\infty} \Big\{ &\left[3\left(|R_{11}(k, \omega)|^2 + |L_1(k, \omega)|^2\right) + 2\Re\left(R_{11}(k, \omega)\overline{L_1(k, \omega)}\right)\right] \cdot h_{F,xx}(k, \omega) \\ &+ |R_{11}(k, \omega) - L_1(k, \omega)|^2 \cdot h_{F,yy}(k, \omega) + 4\,|R_{12}(k, \omega)|^2 \cdot h_{F,zz}(k, \omega) \Big\} \cdot k \, \mathrm{d}k \, , \end{aligned} \tag{7}$$

$$\widetilde{h}_{U,y}(\omega) = \frac{1}{16\pi} \cdot \int_0^{+\infty} \left\{ \left[3\left(|R_{11}(k,\omega)|^2 + |L_1(k,\omega)|^2 \right) + 2\Re\left(R_{11}(k,\omega)\overline{L_1(k,\omega)} \right) \right] \cdot h_{F,yy}(k,\omega) \right.$$
$$\left. + |R_{11}(k,\omega) - L_1(k,\omega)|^2 \cdot h_{F,xx}(k,\omega) + 4\,|R_{12}(k,\omega)|^2 \cdot h_{F,zz}(k,\omega) \right\} \cdot k \ \mathrm{d}k\,, \tag{8}$$

$$\widetilde{h}_{U,z}(\omega) = \frac{1}{4\pi} \cdot \int_0^{+\infty} \left\{ |R_{21}(k,\omega)|^2 \cdot \left[h_{F,xx}(k,\omega) + h_{F,yy}(k,\omega) \right] + 2\,|R_{22}(k,\omega)|^2 \cdot h_{F,zz}(k,\omega) \right\} \cdot k \ \mathrm{d}k\,. \tag{9}$$

In these formulae, functions L_1 and R_{ij} are constructed in terms of propagation matrices and then they contain the mechanical properties of the subsoil stratigraphy.

In order that displacement **U** has a finite frequency power spectrum, it is necessary that the integrands in eqs (7)–(9) are summable in $[0, +\infty[$. Nevertheless, as force and displacement fields are considered at the same depth (the Earth's surface in this case), the terms L_1 and R_{ij} behave as $1/k$ when $k \to +\infty$ (see Appendix B). This prevents convergence of the above power integrals, unless the force power spectral density function itself contributes to the convergence. Thus, the force stochastic field cannot be modelled as 'white noise' with respect to the spatial coordinate **x** and its power spectral density function must be an infinitesimal of order at least $k^{-\epsilon}$ for any $\epsilon > 0$, when $k \to +\infty$. This means that the force field must have a 'colour' relatively to the spatial dimension and this has physical consequences that will be examined in the next section.

3 RELATIONSHIP BETWEEN POWER AND COVARIANCE

The necessity of a dependence of the force power spectral density function on the wavenumber modulus k implies the existence of a spatial correlation of the force field, i.e. a physical relationship between sources located on the Earth's surface. Indeed, the power spectral density function of each jth ($j = x, y, z$) direction is the Fourier transform of the relative covariance function $\mathcal{R}_{F,jj}(\mathbf{x}, t)$ (e.g. Priestley 1981; Vanmarcke 2010):

$$h_{F,jj}(\mathbf{k}, \omega) = \int_{\mathbb{R}^3} \mathcal{R}_{F,jj}(\mathbf{x}, t) \cdot \mathrm{e}^{-\mathrm{i}(\mathbf{k}\mathbf{x} + \omega t)} \ \mathrm{d}\mathbf{x}\,\mathrm{d}t. \tag{10}$$

When expressed in polar coordinates $\mathbf{x} \equiv (r, \vartheta)^{\mathrm{T}}$ and $\mathbf{k} \equiv (k, \phi)^{\mathrm{T}}$, isotropy of the force stochastic field means that $\mathcal{R}_{F,jj}$ is just a function of r and t and implies that

$$h_{F,jj}(k,\omega) = \int_{-\infty}^{+\infty} \left\{ \int_0^{+\infty} \int_0^{2\pi} \mathcal{R}_{F,jj}(r,t) \cdot \mathrm{e}^{-\mathrm{i}kr\cos(\vartheta - \phi) - \mathrm{i}\omega t} \cdot r \ \mathrm{d}r\,\mathrm{d}\vartheta \right\} \mathrm{d}t$$
$$= \int_{-\infty}^{+\infty} \left\{ \int_0^{+\infty} \mathcal{R}_{F,jj}(r,t) \cdot J_0(kr) \cdot r \ dr \right\} \cdot \mathrm{e}^{-\mathrm{i}\omega t} \ \mathrm{d}t \tag{11}$$

for $j = x, y, z$, where J_0 is the zeroth-order Bessel function. This formula states that the power spectral density dependence on the wavenumber modulus is expressed by the zero-order Hankel transform with respect to distance. As the inverse transform has the same structure, it clearly follows that the power spectral density function is isotropic with respect to **k** if and only if the covariance function is isotropic with respect to **x**. That is, isotropy in the wavenumber plane of the force power spectral density function implies that the correlation between sources depends only on their reciprocal distance and vice versa. It is important to stress that this physically plausible hypothesis does not imply isotropy in the intensity of the force field itself: it can act with different intensities along the three Cartesian directions as well.

3.1 Spatio–temporal separability and Gaussian-like spatial covariance

If the covariance function of each component of the force stochastic field is separable, for each $j = x, y, z$, two functions $C_{F,j}(r)$ and $\Theta_{F,j}(t)$ exist, such that $\mathcal{R}_{F,jj}(r,t) = C_{F,j}(r) \cdot \Theta_{F,j}(t)$. In this case, eq. (11) becomes

$$h_{F,jj}(k,\omega) = \left\{ \int_{-\infty}^{+\infty} \Theta_{F,j}(t) \cdot \mathrm{e}^{-\mathrm{i}\omega t} \ \mathrm{d}t \right\} \cdot \left\{ \int_0^{+\infty} C_{F,j}(r) \cdot J_0(kr) \cdot r \ \mathrm{d}r \right\}, \qquad j = x, y, z. \tag{12}$$

This relationship makes sense only if the Fourier-transformability of $\Theta_{F,j}$ and the Hankel-transformability of $C_{F,j}$ hold. Furthermore, in order that the displacement frequency power spectrum is finite, the Hankel transform of each $C_{F,j}$ must converge in k, according to considerations in Section 2. Separability of the covariance function implies that $h_{F,jj}$ is also separable, in terms of two functions depending on the wavenumber modulus k and the angular frequency ω, respectively.

A possible form for the covariance relative to the space domain is a (two-dimensional) Gaussian-like function

$$C_{F,j}(r) = \frac{D_j}{2\pi d_j^2} \cdot \mathrm{e}^{-r^2/(2d_j^2)}, \tag{13}$$

with D_j and d_j being two positive constants, for $j = x, y, z$. Although it is an arbitrary choice, this function is everywhere continuous and infinitely derivable and is physically reasonable, since it implies that the spatial correlation between a couple of sources decreases smoothly with their reciprocal distance.

Naming the Fourier transform of $\Theta_{F,j}(t)$ as $\widehat{\Theta}_{F,j}(\omega)$, the wavenumber–frequency power spectral density of the jth component of the force field is (e.g. eqs 8.411(7) and 6.631(4) of Gradshteyn & Ryzhik 2000)

$$\begin{aligned} h_{F,jj}(k,\omega) &= \widehat{\Theta}_{F,j}(\omega)\cdot\frac{D_j}{2\pi d_j^2}\cdot\int_{-\infty}^{+\infty}\int_{-\infty}^{+\infty}\mathrm{e}^{-(x^2+y^2)/(2d_j^2)}\cdot\mathrm{e}^{-\mathrm{i}\left(k_x x+k_y y\right)}\,\mathrm{d}x\,\mathrm{d}y \\ &= \widehat{\Theta}_{F,j}(\omega)\cdot\frac{D_j}{2\pi d_j^2}\cdot\int_{0}^{+\infty}\int_{0}^{2\pi}\mathrm{e}^{-r^2/(2d_j^2)}\cdot\mathrm{e}^{-\mathrm{i}kr\cos(\vartheta-\phi)}\cdot r\,\mathrm{d}r\,\mathrm{d}\vartheta \\ &= \widehat{\Theta}_{F,j}(\omega)\cdot\frac{D_j}{2\pi d_j^2}\cdot 2\pi\cdot\int_{0}^{+\infty}\mathrm{e}^{-r^2/(2d_j^2)}\cdot J_0(kr)\cdot r\,\mathrm{d}r = \widehat{\Theta}_{F,j}(\omega)\cdot D_j\cdot\mathrm{e}^{-d_j^2\cdot k^2/2}\,, \end{aligned} \tag{14}$$

i.e. the wavenumber part of the power spectral density is the Hankel transform of the spatial part of the covariance. It assumes the form of another Gaussian-like function, which fulfils the decreasing condition necessary to make the displacement frequency power spectrum finite. It is worth noting that, as a consequence of the separability hypothesis, this correlation strength and this power distribution with wavenumber are the same for all frequencies.

For each $j = x, y, z$, the parameter d_j plays the role of a 'correlation range', controlling the form of both the covariance and the power spectral density: large values of this parameter imply long-range correlation between the sources and a contraction of the power spectral density around $k = 0$, i.e. at long wavelengths. This implies that a source covariance function of this kind acts as a high-pass filter in the wavelength domain. For example, the spatial correlation between two sources drops to less than 1 per cent of their variance when their distance is more than $d_j\cdot\sqrt{2\log 100}\simeq 3d_j$. Analogously, more than 99 per cent of the source spectral power at each frequency is given by wavenumbers not greater than about $(1/d_j)\cdot\sqrt{2\log 100}\simeq(3/d_j)$, i.e. wavelengths greater than about $(2\pi)/(3/d_j)\simeq 2.1\cdot d_j$. The possibility of an easy identification of a wavenumber value such that most of the force power is contained in wavenumbers not greater than this allows an optimization in numerical evaluation of the integrals in eqs (7)–(9). Indeed, a suitable k step and k maximum can be chosen on a physical basis and this can make numerical computations faster than in alternative formulations of the problem.

The parameter D_j controls the amplitude of the wavenumber part of the force-field power spectral density function.

The frequency power spectrum of the jth ($j = x, y, z$) component of the force stochastic field, at every angular frequency ω, is obtained by integrating its power spectral density function on the wavenumber plane (e.g. eq. 3.321(3) of Gradshteyn & Ryzhik 2000):

$$\begin{aligned} \widetilde{h}_{F,j}(\omega) &= \frac{1}{(2\pi)^2}\cdot\int_0^{+\infty}\int_0^{2\pi}h_{F,jj}(k,\omega)\cdot k\;\mathrm{d}k\,\mathrm{d}\vartheta = \frac{1}{(2\pi)^2}\cdot\int_{-\infty}^{+\infty}\int_{-\infty}^{+\infty}D_j\cdot\mathrm{e}^{-d_j^2\cdot\left(k_x^2+k_y^2\right)/2}\cdot\widehat{\Theta}_{F,j}(\omega)\;\mathrm{d}k_x\,\mathrm{d}k_y \\ &= \frac{D_j\cdot\widehat{\Theta}_{F,j}(\omega)}{(2\pi)^2}\cdot\left\{\int_{-\infty}^{+\infty}\mathrm{e}^{-d_j^2\cdot k_x^2/2}\;\mathrm{d}k_x\right\}^2 = \frac{D_j\cdot\widehat{\Theta}_{F,j}(\omega)}{(2\pi)^2}\cdot\frac{2\pi}{d_j^2} = \frac{D_j}{2\pi d_j^2}\cdot\widehat{\Theta}_{F,j}(\omega) = C_{F,j}(0)\cdot\widehat{\Theta}_{F,j}(\omega)\,. \end{aligned} \tag{15}$$

Finally, the total power of this force-field component is

$$\frac{1}{2\pi}\cdot\int_{-\infty}^{+\infty}\widetilde{h}_{F,j}(\omega)\,\mathrm{d}\omega = \frac{D_j}{2\pi d_j^2}\cdot\frac{1}{2\pi}\cdot\int_{-\infty}^{+\infty}\widehat{\Theta}_{F,j}(\omega)\,\mathrm{d}\omega = \frac{D_j}{2\pi d_j^2}\cdot\Theta_{F,j}(0) = \mathcal{R}_{F,jj}(0,0)\,, \tag{16}$$

which is the variance of the jth component of the force stochastic field and depends on the parameter ratio D_j/d_j^2.

The shape of the spatial part of the force correlation function [i.e. the normalized force covariance function $C_{F,j}(r)/C_{F,j}(0)$] and the relevant power spectral density function at any frequency $\omega/(2\pi)$, normalized to its value at $k = 0$, are shown in Fig. 1 for different values of the parameter d_j. This spatial correlation can be interpreted physically as representing the interaction of neighbouring point-like sources and/or as the spatial extension of the sources.

It can be useful to note that, in the *Système International d'unités* (SI), the force power spectral density function $h_{F,jj}$ is measured in $\mathrm{N^2\,m^2\,s}$ and the marginal power $\widetilde{h}_{F,j}$ in $\mathrm{N^2\,s = N^2\,Hz^{-1}}$. Then the total force power given by eq. (16) is measured in $\mathrm{N^2}$ and it is natural to interpret its square root as the average force strength per unit surface and time (cf. e.g. Priestley 1981). Analogous interpretations hold for the corresponding quantities relative to the displacement, so $h_{U,jj}$ is measured in $\mathrm{m^4\,s}$ and $\widetilde{h}_{U,j}$ in $\mathrm{m^2\,s = m^2\,Hz^{-1}}$.

4 THE HORIZONTAL-TO-VERTICAL SPECTRAL RATIO

By considering the above formulation, a theoretical representation of the HVSR curve can be obtained. Observing that

$$|R_{11}-L_1|^2 = |R_{11}|^2+|L_1|^2-2\Re\left(R_{11}\overline{L_1}\right),$$

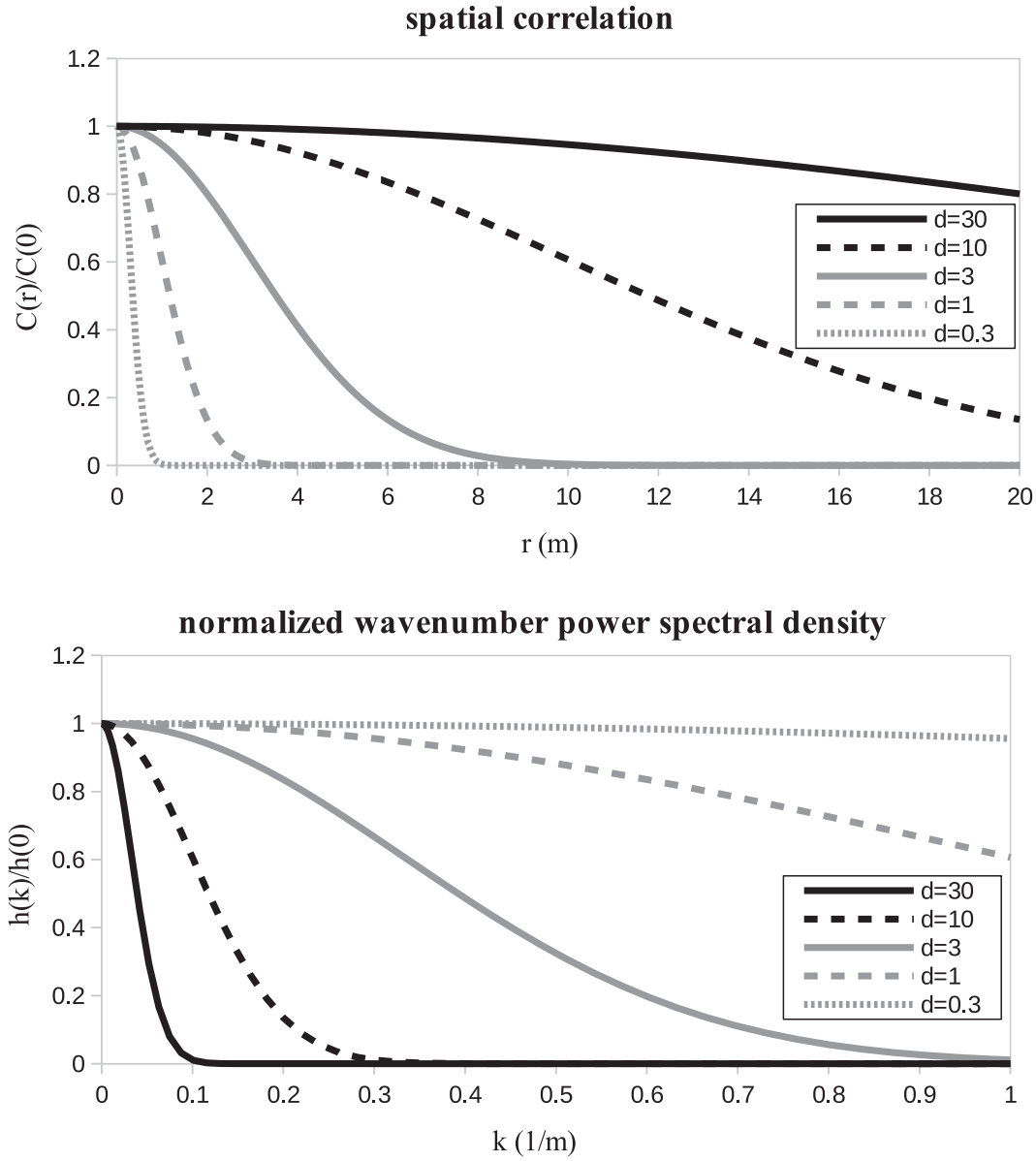

Figure 1. The Gaussian-like force-field spatial correlation function and the corresponding normalized wavenumber part of the power spectral density function for different values of the parameter d, which represents each of the parameters d_x, d_y and d_z.

and using eqs (7) and (8), the spectral power at any angular frequency ω of the horizontal component of displacement can be defined as

$$\begin{aligned} P_H(\omega) &\equiv \widetilde{h}_{U,x}(\omega) + \widetilde{h}_{U,y}(\omega) \\ &= \frac{1}{16\pi} \cdot \int_0^{+\infty} \left\{ 4\left[|R_{11}(k,\omega)|^2 + |L_1(k,\omega)|^2 \right] \cdot h_{F,xx}(k,\omega) + 4\left[|R_{11}(k,\omega)|^2 + |L_1(k,\omega)|^2 \right] \cdot h_{F,yy}(k,\omega) \right. \\ &\quad \left. + 8\,|R_{12}(k,\omega)|^2 \cdot h_{F,zz}(k,\omega) \right\} \cdot k \ \mathrm{d}k \\ &= \frac{1}{4\pi} \cdot \int_0^{+\infty} \left\{ \left[|R_{11}(k,\omega)|^2 + |L_1(k,\omega)|^2 \right] \cdot \left[h_{F,xx}(k,\omega) + h_{F,yy}(k,\omega) \right] + 2\,|R_{12}(k,\omega)|^2 \cdot h_{F,zz}(k,\omega) \right\} \cdot k \ \mathrm{d}k \,. \end{aligned} \tag{17}$$

The vertical spectral power is instead directly given by eq. (9):

$$\begin{aligned} P_V(\omega) &\equiv \widetilde{h}_{U,z}(\omega) \\ &= \frac{1}{4\pi} \cdot \int_0^{+\infty} \left\{ |R_{21}(k,\omega)|^2 \cdot \left[h_{F,xx}(k,\omega) + h_{F,yy}(k,\omega) \right] + 2\,|R_{22}(k,\omega)|^2 \cdot h_{F,zz}(k,\omega) \right\} \cdot k \ \mathrm{d}k \,. \end{aligned} \tag{18}$$

The HVSR can be then computed as

$$HV(\omega) \equiv \sqrt{\frac{P_H(\omega)}{P_V(\omega)}}. \tag{19}$$

It is important to remark that, under the hypothesis of a Gaussian-like force-field spatial covariance given by eq. (13), the curve $HV(\omega)$ does not depend on the parameters D_j nor on the functions $\widehat{\Theta}_{F,j}(\omega)$, but just on the parameters d_j, which determine the shape of the force spatial correlation and power spectral density. In other words, it depends only on the spatial correlation of the force field, i.e. on the relative power distribution between the wavenumbers (or wavelengths).

5 A NUMERICAL EXAMPLE

The results of the previous sections allow us to obtain a synthetic HVSR curve for any established stratigraphical profile. To show how the proposed formalization works, a synthetic HVSR curve has been computed by considering the subsoil profile A used in Tokimatsu (1997), Arai & Tokimatsu (2004) and Lunedei & Albarello (2009), which is shown in in Table 1. Differently from the latter, here all the damping factors are assumed equal to 1 per cent. Viscosity is included in the quoted integrals by assuming the equivalence principle, i.e. by making body wave velocities complex and dispersive in the form

$$\frac{V_\gamma}{1-(2\cdot D_\gamma/\pi)\cdot\log(\omega/\omega_{\rm ref})}\cdot\left[1-\mathrm{i}D_\gamma\right], \qquad \gamma = P, S,$$

where $\omega_{\rm ref}/(2\pi)$ is the material reference frequency, here fixed, as usual, equal to 1 Hz (see, e.g. Lunedei & Albarello 2009).

Results are shown in the bottom panel of Fig. 2 for values of d (which is the common value of d_x, d_y and d_z) ranging between 0.3 and 30. The top and medium panels show the effect of changing d on the displacement frequency power spectra P_H and P_V, with $D_x = D_y = D_z = 1/3$. One can see that the resulting HVSR and frequency power spectrum curves remain practically unchanged when d decreases below 3. However, above this value the shape of the HVSR changes significantly: the HVSR peak shifts towards lower frequencies and a number of secondary peaks appear, the amplitudes of which increase with d. This is not a numerical effect and indicates some physical effect due to the correlation range. This suggests a possible constraint on the source-field characteristics adopted for modelling the HVSR curve. In fact, experimental practice shows the lack of strong secondary peaks in HVSR curves and this suggests that short-range correlation should generally characterize the ambient vibration sources. Changes in the HVSR curve reflect those in the power-spectrum curves, for which a major sensitivity to the correlation range arises for frequencies lower and higher than the HVSR peak. As expected, the computational speed increases along with d.

Fig. 2 clearly shows that, for this particular example, the parameter threshold at which the HVSR curve changes its overall shape is located between 3 and 10. Therefore the value $d = 3$ has been chosen as a reference, to compare the outcomes of this new model with the ones provided by alternative models applied to the same stratigraphy: the HVSR curves obtained are shown in Fig. 3. Four alternative models are considered here: two full-wavefield models (the DFA by Sánchez-Sesma *et al.* 2011 and the DSS in the form proposed by Lunedei & Albarello 2010), the surface wave approximation presented in Lunedei & Albarello (2009) and the vertically incident body wave approximation proposed by Herak (2008). It clearly emerges that, despite the significant differences in the underlying physical hypotheses, all the full-wavefield models provide similar results. The surface wave approximation provides a significant shift in frequency (of about 25 per cent) and rise in amplitude (up to 50 per cent) of the HVSR main peak with respect to the other results. The vertically incident body wave approximation produces a very different pattern including a number of secondary peaks, the envelope of which, however, mimics (quite roughly) the HVSR-curve patterns provided by the full-wavefield models.

Table 1. Seismic stratigraphy used in the numerical example.

H (m)	V_P (m s^{-1})	V_S (m s^{-1})	ρ (kg m^{-3})	D_P (%)	D_S (%)
5.5	1333	240	1900	1	1
3.6	1333	133	1900	1	1
4.6	1333	175	1900	1	1
6.3	1333	222	1900	1	1
20.0	1333	155	1900	1	1
4.6	1333	175	1900	1	1
6.4	1333	250	1900	1	1
9.0	1595	570	1900	1	1
23.6	1595	333	1900	1	1
16.4	1595	575	1900	1	1
1400.0	1800	700	1900	1	1
800.0	2800	1500	2200	1	1
∞	5600	3000	2500	1	1

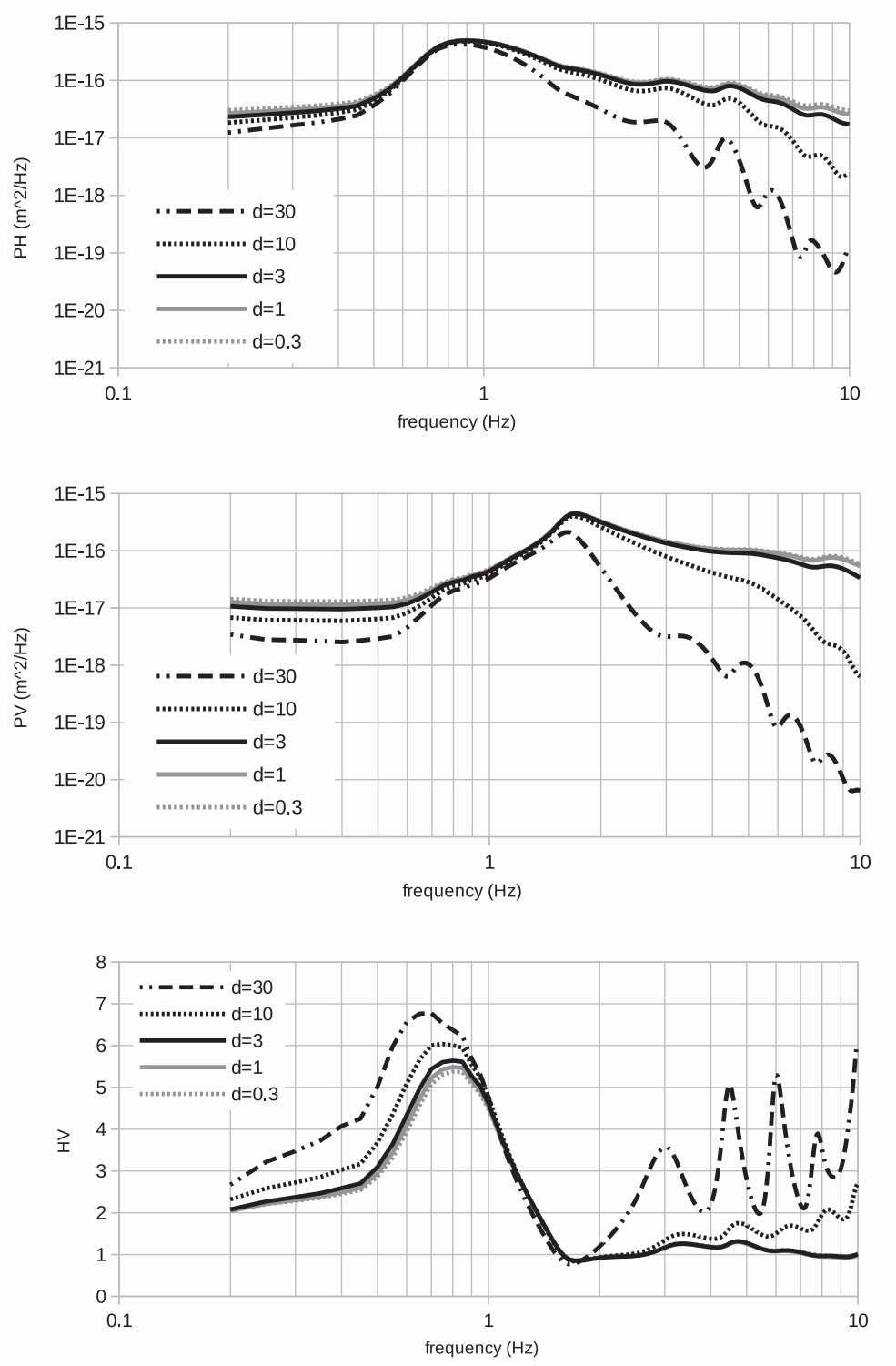

Figure 2. Frequency power spectra of the horizontal (P_H; top panel) and vertical (P_V; middle panel) ground-motion displacement and relative HVSR curve (*HV*; bottom panel), for the stratigraphical profile in Table 1. Curves are obtained using the model presented in this article and are relative to different values of the parameter *d*.

6 AN EXPERIMENTAL CASE

In order to evaluate the possibility of practical use of the proposed theory in real situations, the site of the Mirandola's strong-motion station (belonging to the Italian accelerometric network, RAN) is considered here. Near this station, an experimental HVSR curve was

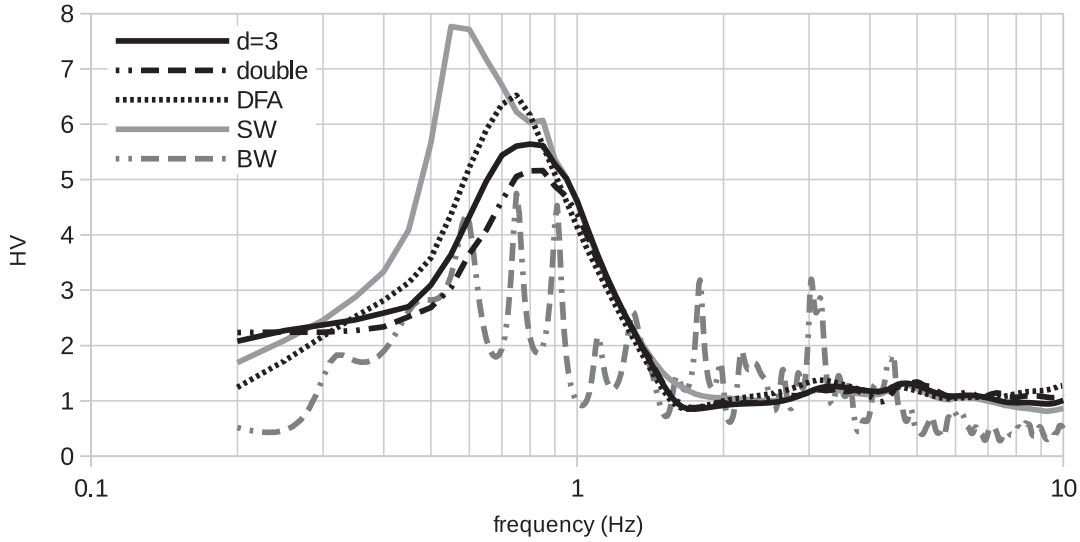

Figure 3. HVSR curves for the stratigraphical profile in Table 1 produced by the present model with $d = 3$ and by other models: the spatial–wavenumber integration method (Lunedei & Albarello 2010; marked by 'double'), the DFA model (Sánchez-Sesma *et al.* 2011), the surface wave based model (Lunedei & Albarello 2009; 'SW') and the vertically incident body wave model (Herak 2008; 'BW').

Table 2. Simplified stratigraphy describing the Mirandola RAN site.

H	V_P	V_S	ρ	First group		Second group	
(m)	(m s^{-1})	(m s^{-1})	(kg m^{-3})	D_P	D_S	D_P	D_S
2	640	170	1500	0.020	0.020	0.045	0.045
2	770	170	1500	0.015	0.015	0.045	0.045
2	940	180	1500	0.010	0.010	0.040	0.040
4	1360	200	1500	0.005	0.005	0.040	0.040
2	1770	210	2000	0.001	0.001	0.035	0.035
10	1740	210	2000	0.001	0.001	0.030	0.030
2	1760	230	2000	0.001	0.001	0.025	0.025
2	1820	260	2000	0.001	0.001	0.025	0.025
2	1760	280	2000	0.001	0.001	0.025	0.025
4	1790	290	2000	0.001	0.001	0.020	0.020
2	1820	300	2000	0.001	0.001	0.015	0.015
2	1840	320	2000	0.001	0.001	0.015	0.015
2	1840	340	2000	0.001	0.001	0.010	0.010
3	1860	350	2000	0.001	0.001	0.010	0.010
9	1890	330	2000	0.001	0.001	0.005	0.005
3	1890	330	2000	0.001	0.001	0.004	0.004
4	1940	360	2100	0.001	0.001	0.004	0.004
3	1960	420	2100	0.001	0.001	0.003	0.003
4	2030	410	2100	0.001	0.001	0.003	0.003
6	2000	350	2100	0.001	0.001	0.002	0.002
3	1920	350	2100	0.001	0.001	0.002	0.002
2	2000	410	2100	0.001	0.001	0.001	0.001
12	2110	430	2100	0.001	0.001	0.001	0.001
9	2160	410	2100	0.001	0.001	0.001	0.001
6	2170	510	2100	0.001	0.001	0.001	0.001
8	2290	440	2100	0.001	0.001	0.001	0.001
5	2560	530	2200	0.001	0.001	0.001	0.001
3	2810	740	2300	0.001	0.001	0.001	0.001
∞	3170	860	2300	0.001	0.001	0.001	0.001

obtained from ambient vibrations. The measurement was carried out by a tri-directional digital tromograph Tromino® Micromed (see www.tromino.eu), with a sampling frequency of 128 Hz and an acquisition time length of 30 min, and processed according to the guidelines provided by SESAME (2004) and other studies (see e.g. Picozzi *et al.* 2005). At the same site, a cross-hole test has been also performed by providing *P*- and *S*-wave velocity values up to a depth of 125 m. We simplified the resulting *P*- and *S*-wave velocity profiles, obtaining the values in Table 2. Bulk densities have not been provided by the cross-hole test and thus we fixed a value of 1500 kg m^{-3} whenever the V_P value is not higher than 1500 m s^{-1} and equal to $1740 \cdot (V_P/1000)^{0.25}$ kg m^{-3} (rounded at 100 kg m^{-3}) with V_P in m s^{-1} otherwise

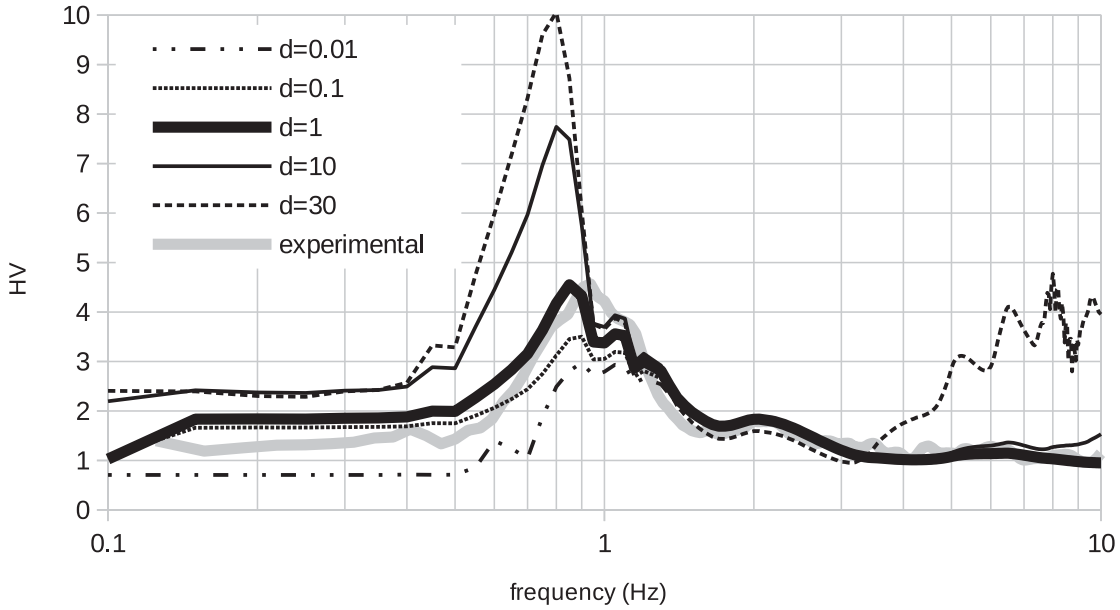

Figure 4. HVSR curves for the stratigraphical profile in Table 2 with damping values of the first group, produced by the present model with different values of d.

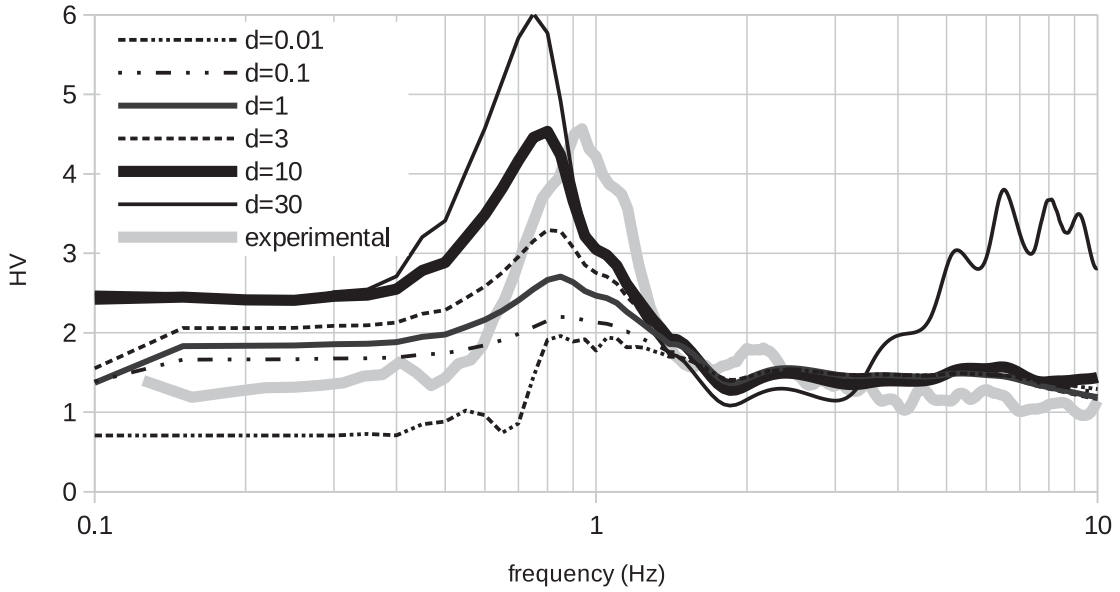

Figure 5. HVSR curves for the stratigraphical profile in Table 2 with damping values of the second group, produced by the present model with different values of d.

(see http://daveboore.com/daves_notes/daves_notes_on_relating_density_to_velocity_v1.2.pdf; Gardner *et al.* 1974). No estimate is available about material damping relative to P and S waves at the very low strain levels of concern here (some laboratory results generically valid for a wide area are given in Martelli *et al.* 2014). As the viscosity can influence the HVSR peak amplitude, this implies that suitable values must be deduced in order that the experimental HVSR curve can be reproduced by the numerical one. To complicate this task, a trade-off between these values and the spatial correlation parameters d_j ($j = x, y, z$) emerged in our tests. To cope with this situation, a two-step procedure has been adopted.

As a first step, two values for the spatial correlation parameter d, which represents the common value for the three parameters d_x, d_y and d_z, have been fixed initially. For each of these two values, a set of damping factors D_P and D_S has been chosen, such that the synthetic HVSR curve was as close as possible to the experimental one. These sets of values are reported in Table 2: the first group is the best-fitting set for $d = 1$, while the second group is the corresponding one for $d = 10$. As a second step, for each of the two damping profiles obtained in this way, different values of the common spatial correlation parameter d have been tested: the results are shown in Figs 4 and 5. We note that, in order to follow the definition used for the experimental HVSR curve, all curves shown in these last two figures are defined by dividing the right-hand side of eq. (19) by $\sqrt{2}$.

First of all, these results indicate that the model is able to reproduce the experimental HVSR curve satisfactorily starting from the known (in velocity values only) seismo-stratigraphic profile. Differences in the peak position, less than 0.09 Hz for the first-group best result and less than 0.14 Hz for the second-group one, however, can depend on the unknown density and viscosity values as well as on the model. In spite of the fact that the damping values in the second group are closer to those that laboratory tests estimated for the materials in that zone (cf. Martelli *et al.* 2014), the corresponding theoretical HVSR curve reproduces the experimental one in a worse way.

It is important to highlight that this example does not show a rigorous inversion of the experimental datum by means of the new model, which would be too cumbersome a task with the current numerical performance of this model. We simply aim to show that application to real situations is possible and that such application could also contribute to establishing admissible ranges for the model parameters. Indeed, in this example, as in the numerical one of Section 5, Figs 4 and 5 show clearly that the pattern of the synthetic HVSR curve is significantly affected by the d value. Furthermore, in order to obtain HVSR curves compatible with the experimental one, d must lie within the relatively narrow range [0.01,30] m, irrespective of the values of damping factors adopted in the simulations. These values for d imply that the force-field spatial correlation should extend approximately from a few cm to less than 100 m. The lower limit of this correlation extension is established in a less precise way, as numerical instabilities seem to appear in the relative HVSR curves, but its size order describes a situation not very different, from a practical point of view, from a system of point-like uncorrelated sources. So, possible numerical effects appearing for this d value do not seem very important for the practical use of the model, although they are deserving of further careful investigation.

This example, even though it is obviously not sufficient to find a best value for the parameter d, clearly suggests that this parameter cannot take any value, but, on the contrary, should be confined in a rather small interval.

7 CONCLUSIONS

A new version of the distributed surface sources (DSS) model of the ambient vibration full wavefield is presented in this article. The key hypotheses on which this model relies are as follows.

(1) The ground displacement and the sources are two stochastic fields (in time and position on the Earth's surface), which are homogeneous in all their variables, have zero mean and finite variance and can be characterized in terms of the respective power spectral density functions.
(2) These two fields are linearly related via the Green's function, describing the effect of the subsoil on the seismic wave propagation.
(3) The three Cartesian components of the force field are mutually uncorrelated and their spatial covariances are isotropic in the horizontal plane.
(4) The power spectral density function of the force field is separable in its frequency and wavenumber dependences.

Under these hypotheses, the frequency power spectrum of each component of the displacement due to the ambient vibrations can be computed by a single integration in the wavenumber domain. As a consequence, the synthetic HVSR curve for the ambient vibration full wavefield is obtained with an effectiveness comparable with the one of the alternative model, based on the hypothesis that ambient vibrations are a diffuse wavefield (the DFA model). Moreover, the physically unrealistic assumption that all the sources are point-like and spatially uncorrelated one another, on which the previous DSS model relies (Lunedei & Albarello 2010), is released, so also warranting the convergence of the integrations in the wavenumber domain.

A possible form for the force-field spatial covariance has been introduced, which is computationally effective and physically plausible. A couple of parameters control this form and one of them determines the correlation range, i.e. the distance beyond which correlation becomes negligible. This range can be physically interpreted as the distance at which dynamical source-to-source interaction vanishes and/or the finite spatial extension of the sources responsible for the ambient vibration wavefield. The adopted covariance acts as a low-pass filter in the wavenumber domain, i.e. as a high-pass filter in the wavelength domain, for the forces generating the ambient vibration wavefield. A consequence of this fact is that most of the force power is contained in a finite range of wavenumbers and this allows an optimization in the numerical evaluation of displacement power integrals built up on a physical basis and not just through numerical analysis techniques. Moreover, the computational speed is also influenced by the parameter that defines the correlation range, because they increase together. On the other hand, this parameter plays a role in determining the overall shape of the synthetic HVSR curve and this implies that experimental observations under controlled conditions (a well-known subsoil configuration) might, in principle, allow us to constrain the correct shape for the force-field covariance function.

A weak point of the model presented here is a consequence of the assumed separability of the force power spectral density function in wavenumber and frequency contributions, which implies that no relationship exists between space and time characteristics of sources. This is probably unrealistic, since one can expect that ambient vibration low-frequency sources (mainly related to large-scale meteoclimatic conditions) are characterized by larger wavelengths with respect to high-frequency sources. Experimental data might help us to evaluate to what extent this approximation is able to provide realistic results.

Two examples of application of this new model have also been examined. In the first of them, for a given subsoil profile, the role of the force correlation-range parameter in affecting the outcomes is exemplified. Moreover, a comparison with other models is shown. The HVSR curve produced by the present new model is in line with those given by the other full-wavefield ones, the previous versions of the DSS and DFA models, irrespective of the underlying different physical hypotheses. Despite the fact that less refined models (based on body or surface wave approximations) also provide results that roughly mimic the shape provided by most refined models, significant differences exist, suggesting caution when such models are considered for the inversion of experimental HVSR curves. These comparisons also suggest

that the overall shape of the HVSR curve could be relatively 'robust' with respect to the adopted simulation model, since, in the example considered, the salient features of this curve are reproduced by all the models considered, although founded on different physical hypotheses. This surprising fact might be due to the pre-eminent role played by the Green's function, which is the main common feature of all the models considered, in determining the overall HVSR pattern.

The second example is a real site, where the HVSR curve and *P*- and *S*-wave velocity profiles are known. The proposed new model, which also includes the separability of time and space correlation properties, has proved able to reproduce an experimental HVSR curve acceptably. It also emerges that, in order that the synthetic HVSR curve is able to reproduce the overall pattern of the experimental one correctly, the force-field correlation range parameter must belong to a certain range of values. Moreover, it seems that this range does not depend strongly on the subsoil viscosity profile, which is a property able to influence the HVSR amplitude. Even more interesting is that the upper-limit value found for the force-field correlation-range parameter is approximately the same as that separating two different groups of overall shape of HVSR curve in the other example mentioned above. This fact seems to suggest that the range of admissible values for the force-field correlation-range parameter is not strongly sensitive to the stratigraphic profile in general. If this were confirmed in a more wide set of cases, the dependence on this parameter, which is another weak point of this new model, could be controlled by finding a suitable relatively narrow range of values admissible for it.

The results given by both numerical and real examples suggest that it might be possible to constrain the shape of the force-field spatial correlation and to establish an acceptable range for model parameter values. This opens up possible prospects for application of this new model, both in characterizing the ambient vibration wavefield properties and in using the full wavefield in inversion procedures. Obviously, the model needs many other tests, as well as further improvement in computing speed.

As other proposals for the future, we note that the model could be made more general by both releasing the separability of time and space dependence of the force correlation function and taking into account some kind of spatial non-homogeneity. Non-separability would allow us to describe the different spatial-correlation extensions at different frequencies. Spatial non-homogeneity would allow us to take into account more complex, hence probably more realistic, structures for the force field generating the ambient vibrations, such as e.g. directional source distributions or source-free areas. This last case could also be interesting, in order to establish whether the lack of convergence of the displacement power-integrals in Lunedei & Albarello (2010) remains in the presence of a source-free area around the receiver, for example.

ACKNOWLEDGEMENTS

The authors thanks Antonio García Jerez (Universidad de Granada) for useful discussions about power integrals. The authors also thank the two anonymous reviewers for their observations, which contributed to improving the article.

REFERENCES

Albarello, D. & Lunedei, E., 2010. Alternative interpretations of Horizontal to Vertical Spectral Ratios of ambient vibrations: new insights from theoretical modeling, *Bull. Earthq. Eng.,* **8**(3), 519–534.

Albarello, D. & Lunedei, E., 2011. Structure of ambient vibration wavefield in the frequency range of engineering interest ([0.5,20] Hz): insights from numerical modelling, *Near Surface Geophysics,* **9,** 543–559.

Albarello, D., Cesi, C., Eulilli, V., Guerrini, F., Lunedei, E., Paolucci, E., Pileggi, D. & Puzzilli, L.M., 2011. The contribution of the ambient vibration prospecting in seismic microzoning: an example from the area damaged by the April 6, 2009 LAquila (Italy) earthquake, *Bollettino di Geofisica Teorica ed Applicata,* **52**(3), 513–538.

Arai, H. & Tokimatsu, K., 2000. Effect of Rayleigh and Love waves on microtremor H/V spectra, in *Proceedings of the 12th World Conferences on Earthquake Engineering (WCEE),* Auckland, New Zealand. Available at: http://www.nicee.org/wcee/, last accessed 26 February 2015.

Arai, H. & Tokimatsu, K., 2004. S-wave velocity profiling by inversion of microtremor H/V spectrum, *Bull. seism. Soc. Am.,* **94**(1), 53–63.

Bard, P.Y., 1998. Microtremor measurements: a tool for site effect estimation?, in *Proceedings of the 2nd Int. Symposium on the Effects of Surface Geology on Seismic Motion,* Yokohama, Japan, 1251–1279.

Bonnefoy-Claudet, S. *et al.*, 2004. Simulation of seismic ambient noise: I. Results of H/V and array techniques on canonocal models, in *Proceedings of the 13th World Conferences on Earthquake Engineering (WCEE),* Vancouver, Canada. Available at: http://www.nicee.org/wcee/, last accessed 26 February 2015.

Bonnefoy-Claudet, S., Cornou, C., Bard, P.Y., Cotton, F., Moczo, P., Kristek, J. & Fäh, D., 2006. H/V ratio: a tool for site effects evaluation. Results form 1-D noise simulation, *Geophys. J. Int.,* **167,** 827–837.

Bonnefoy-Claudet, S., Köhler, A., Cornou, C., Wathelet, M. & Bard, P.Y., 2008. Effects of Love waves on microtremor H/V ratio, *Bull. seism. Soc. Am.,* **98**(1), 288–300.

Castellaro, S. & Mulargia, F., 2009. V_{S30} estimates using constrained H/V measurements, *Bull. seism. Soc. Am.,* **99**(2A), 761–773.

Field, E. & Jacob, K., 1993. The theoretical response of sedimentary layers to ambient seismic noise, *Geophys. Res. Lett.,* **20**(24), 2925–2928.

García-Jerez, A., Luzón, F., Albarello, D., Lunedei, E., Santoyo, M.A., Margerin, L. & Sánchez-Sesma, F.J., 2012. Comparison between ambient vibrations H/V obtained from the diffuse field and distributed durface source models, in *Proceedings of the 15th World Conferences on Earthquake Engineering (WCEE),* 24–28 September, Lisbon, Portugal. Available at: http://www.nicee.org/wcee/, last accessed 26 February 2015.

Gardner, G.H.F., Gardner, L.W. & Gregory, A.R., 1974. Formation velocity and density the diagnostic basics for stratigraphic traps, *Geophysics,* **39**(6), 770–780.

Gradshteyn, I.S. & Ryzhik, I.M., 2000. *Table of Integrals, Series, and Products*, 6th edn, Academic Press.

Herak, M., 2008. ModelHVSR – A Matlab tool to model horizontal-to-vertical spectral ratio of ambient noise, *Computers & Geosciences,* **34**(11), 1514–1526.

Hisada, Y., 1994. An efficient method for computing Green's functions for a layered half-space with sources and receivers at close depths, *Bull. seism. Soc. Am.,* **84**(5), 1456–1472.

Lanchet, C. & Bard, P.Y., 1994. Numerical and theoretical investigations on the possibilities and limitations of Nakamura's technique, *J. Phys. Earth,* **42,** 377–397.

Lunedei, E. & Albarello, D., 2009. On the seismic noise wave field in a weakly dissipative layered Earth, *Geophys. J. Int.,* **177**(3), 1001–1014, doi: 10.1111/j.1365 246X.2008.04062.x (Erratum doi:10.1111/j.1365-246X.2009.04344.x).

Lunedei, E. & Albarello, D., 2010. Theoretical HVSR from the full wave field modelling of ambient vibrations in a weakly dissipative layered Earth, *Geophys. J. Int.,* **181,** 1093–1108.

Martelli, L. *et al.*, 2014. Analysis of the local seismic hazard for the stability tests of the main bank of the Po River (northern Italy), *Bollettino di Geofisica Teorica ed Applicata,* **55**(1), 119–134.

Okada, H., 2003. *The Microtremor Survey Method* (Geophysical Monograph Series No. 12), Society of Exploration Geophysicists, 135 pp.

Parolai, S., 2014. Shear wave quality factor Qs profiling using seismic noise data from microarrays, *J. Seismol.,* **18,** 695–704.

Picozzi, M. & Albarello, D., 2007. Combining genetic and linearized algorithms for a two-step joint inversion of Rayleigh wave dispersion and H/V spectral ratio curves, *Geophys. J. Int.,* **169,** 189–200.

Picozzi, M., Parolai, S. & Albarello, D., 2005. Statistical analysis of Horizontal to Vertical Spectral Ratios (HVSR), *Bull. seism. Soc. Am.,* **95**(5), 1779–1786.

Priestley, M.B., 1981. *Spectral Analysis and Time Series,* Academic Press.

Sánchez-Sesma, F.J. *et al.*, 2011. A theory for microtremor H/V spectral ratio: application for a layered medium, *Geophys. J. Int.,* **186,** 221–225.

SESAME, 2004. *Guidelines for the Implementation of the H/V Spectral Ratio Technique on Ambient Vibrations*, SESAME, European project, WP12, Deliverable D23.12.

Tokimatsu, K., 1997. Geotechnical site characterization using surface waves, in *Earthquake Geotechnical Engineering: Proceedings of IS-Tokyo '95, the First International Conference on Earthquake Geotechnical Engineering, Tokyo,* 14–16 November, 1995, pp. 1333–1368, ed. Ishihara, K., A A Balkema.

Vanmarcke, E., 2010. *Random fields – Analysis and Synthesis* (revised and expanded new edn), World Scientific Publishing.

APPENDIX A: DISPLACEMENT FREQUENCY POWER-SPECTRUM COMPONENTS

By using the expressions for the Green's matrix entries given in Appendix B, under the hypothesis of isotropy in the wavenumber plane for the force power spectral density function, a straightforward computation shows that the components defined in eq. (6) take the following form:

$$\begin{aligned}
\mathfrak{h}_{xx}(\omega) &= \frac{1}{(2\pi)^2}\cdot\int_0^{+\infty}\int_0^{2\pi}\left|R_{11}(k,\omega)\cdot\cos^2\phi + L_1(k,\omega)\cdot\sin^2\phi\right|^2\cdot h_{F,xx}(k,\omega)\cdot k\ \mathrm{d}k\,\mathrm{d}\phi\\
&= \frac{1}{(2\pi)^2}\cdot\int_0^{+\infty}\int_0^{2\pi}\left\{|R_{11}(k,\omega)|^2\cdot\cos^4\phi + R_{11}(k,\omega)\cdot\overline{L_1(k,\omega)}\cdot\cos^2\phi\sin^2\phi\right.\\
&\quad\left.+\,\overline{R_{11}(k,\omega)}\cdot L_1(k,\omega)\cdot\cos^2\phi\sin^2\phi + |L_1(k,\omega)|^2\cdot\sin^4\phi\right\}\cdot h_{F,xx}(k,\omega)\cdot k\ \mathrm{d}k\,\mathrm{d}\phi\\
&= \frac{1}{(2\pi)^2}\cdot\int_0^{+\infty}\left\{|R_{11}(k,\omega)|^2\,\frac{3}{4}\pi + 2\Re\left(R_{11}(k,\omega)\overline{L_1(k,\omega)}\right)\cdot\frac{\pi}{4} + |L_1(k,\omega)|^2\,\frac{3}{4}\pi\right\}\cdot h_{F,xx}(k,\omega)\cdot k\ \mathrm{d}k\\
&= \frac{1}{16\pi}\cdot\int_0^{+\infty}\left\{3\left[|R_{11}(k,\omega)|^2 + |L_1(k,\omega)|^2\right] + 2\Re\left(R_{11}(k,\omega)\overline{L_1(k,\omega)}\right)\right\}\cdot h_{F,xx}(k,\omega)\cdot k\ \mathrm{d}k\,,
\end{aligned}$$

$$\begin{aligned}
\mathfrak{h}_{xy}(\omega) &= \frac{1}{(2\pi)^2}\cdot\int_0^{+\infty}\int_0^{2\pi}|R_{11}(k,\omega) - L_1(k,\omega)|^2\cdot\cos^2\phi\sin^2\phi\cdot h_{F,yy}(k,\omega)\cdot k\ \mathrm{d}k\,\mathrm{d}\phi\\
&= \frac{1}{16\pi}\cdot\int_0^{+\infty}|R_{11}(k,\omega) - L_1(k,\omega)|^2\cdot h_{F,yy}(k,\omega)\cdot k\ \mathrm{d}k\,,
\end{aligned}$$

$$\begin{aligned}
\mathfrak{h}_{xz}(\omega) &= \frac{1}{(2\pi)^2}\cdot\int_0^{+\infty}\int_0^{2\pi}|R_{12}(k,\omega)|^2\cdot\cos^2\phi\cdot h_{F,zz}(k,\omega)\cdot k\ \mathrm{d}k\,\mathrm{d}\phi\\
&= \frac{1}{4\pi}\cdot\int_0^{+\infty}|R_{12}(k,\omega)|^2\cdot h_{F,zz}(k,\omega)\cdot k\ \mathrm{d}k\,,
\end{aligned}$$

$$\begin{aligned}
\mathfrak{h}_{yx}(\omega) &= \frac{1}{(2\pi)^2}\cdot\int_0^{+\infty}\int_0^{2\pi}|R_{11}(k,\omega) - L_1(k,\omega)|^2\cdot\cos^2\phi\sin^2\phi\cdot h_{F,xx}(k,\omega)\cdot k\ \mathrm{d}k\,\mathrm{d}\phi\\
&= \frac{1}{16\pi}\cdot\int_0^{+\infty}|R_{11}(k,\omega) - L_1(k,\omega)|^2\cdot h_{F,xx}(k,\omega)\cdot k\ \mathrm{d}k\,,
\end{aligned}$$

$$\begin{aligned}
\mathfrak{h}_{yy}(\omega) &= \frac{1}{(2\pi)^2}\cdot\int_0^{+\infty}\int_0^{2\pi}\left|R_{11}(k,\omega)\cdot\sin^2\phi + L_1(k,\omega)\cdot\cos^2\phi\right|^2\cdot h_{F,yy}(k,\omega)\cdot k\ \mathrm{d}k\,\mathrm{d}\phi\\
&= \frac{1}{16\pi}\cdot\int_0^{+\infty}\left\{3\left[|R_{11}(k,\omega)|^2 + |L_1(k,\omega)|^2\right] + 2\Re\left(R_{11}(k,\omega)\overline{L_1(k,\omega)}\right)\right\}\cdot h_{F,yy}(k,\omega)\cdot k\ \mathrm{d}k\,,
\end{aligned}$$

$$\mathfrak{h}_{yz}(\omega) = \frac{1}{(2\pi)^2} \cdot \int_0^{+\infty} \int_0^{2\pi} |R_{12}(k,\omega)|^2 \cdot \sin^2\phi \cdot h_{F,zz}(k,\omega) \cdot k \ \mathrm{d}k \, \mathrm{d}\phi$$
$$= \frac{1}{4\pi} \cdot \int_0^{+\infty} |R_{12}(k,\omega)|^2 \cdot h_{F,zz}(k,\omega) \cdot k \ \mathrm{d}k \,,$$

$$\mathfrak{h}_{zx}(\omega) = \frac{1}{(2\pi)^2} \cdot \int_0^{+\infty} \int_0^{2\pi} |R_{21}(k,\omega)|^2 \cdot \cos^2\phi \cdot h_{F,xx}(k,\omega) \cdot k \ \mathrm{d}k \, \mathrm{d}\phi$$
$$= \frac{1}{4\pi} \cdot \int_0^{+\infty} |R_{21}(k,\omega)|^2 \cdot h_{F,xx}(k,\omega) \cdot k \ \mathrm{d}k \,,$$

$$\mathfrak{h}_{zy}(\omega) = \frac{1}{(2\pi)^2} \cdot \int_0^{+\infty} \int_0^{2\pi} |R_{21}(k,\omega)|^2 \cdot \sin^2\phi \cdot h_{F,yy}(k,\omega) \cdot k \ \mathrm{d}k \, \mathrm{d}\phi$$
$$= \frac{1}{4\pi} \cdot \int_0^{+\infty} |R_{21}(k,\omega)|^2 \cdot h_{F,yy}(k,\omega) \cdot k \ \mathrm{d}k,$$

$$\mathfrak{h}_{zz}(\omega) = \frac{1}{(2\pi)^2} \cdot \int_0^{+\infty} \int_0^{2\pi} |R_{22}(k,\omega)|^2 \cdot h_{F,zz}(k,\omega) \cdot k \ \mathrm{d}k \, \mathrm{d}\phi$$
$$= \frac{1}{2\pi} \cdot \int_0^{+\infty} |R_{22}(k,\omega)|^2 \cdot h_{F,zz}(k,\omega) \cdot k \ \mathrm{d}k.$$

APPENDIX B: ENTRIES OF THE GREEN'S MATRIX IN THE WAVENUMBER–FREQUENCY DOMAIN

The entries of the Green's matrix in the wavenumber–frequency domain, given by eq. (3), are a classical result, which can be written, if the wavenumber vector is expressed in polar coordinates $\mathbf{k} \equiv (k, \phi)^{\mathrm{T}}$, as

$$\widehat{G}_{xx}(k,\phi,\omega) = -\left[R_{11}(k,\omega) \cdot \cos^2\phi + L_1(k,\omega) \cdot \sin^2\phi\right],$$

$$\widehat{G}_{xy}(k,\phi,\omega) = -\left[R_{11}(k,\omega) - L_1(k,\omega)\right] \cdot \cos\phi \sin\phi,$$

$$\widehat{G}_{xz}(k,\phi,\omega) = -R_{12}(k,\omega) \cdot \cos\phi,$$

$$\widehat{G}_{yx}(k,\phi,\omega) = -\left[R_{11}(k,\omega) - L_1(k,\omega)\right] \cdot \cos\phi \sin\phi,$$

$$\widehat{G}_{yy}(k,\phi,\omega) = -\left[R_{11}(k,\omega) \cdot \sin^2\phi + L_1(k,\omega) \cdot \cos^2\phi\right],$$

$$\widehat{G}_{yz}(k,\phi,\omega) = -R_{12}(k,\omega) \cdot \sin\phi,$$

$$\widehat{G}_{zx}(k,\phi,\omega) = \mathrm{i} \cdot R_{21}(k,\omega) \cdot \cos\phi,$$

$$\widehat{G}_{zy}(k,\phi,\omega) = \mathrm{i} \cdot R_{21}(k,\omega) \cdot \sin\phi,$$

$$\widehat{G}_{zz}(k,\phi,\omega) = \mathrm{i} \cdot R_{22}(k,\omega).$$

Functions L_1 and R_{ij}, which do not depend on ϕ, are constructed by the propagation matrices in the stratified medium and contain all the information about the mechanical properties of the subsoil. Their expressions can be found in appendix A of Lunedei & Albarello (2010), where in the formula defining L_H (penultimate equation on the left side of p. 1106) the denominator $F_L(k)$ is missing because of a misprint. These functions are similar to the coefficients H and V in Hisada (1994), from which they differ by a factor of k and some constants. By using the results exposed in appendix B of Hisada (1994) when the observation point and the source point are at the same quote, it is possible to conclude that leading terms of the functions L_1 and R_{ij} behave as $1/k$ as k goes toward infinity.